Conveniently controllable design of nano-Al-doped@Co₃O₄ energetic composite with enhanced exothermic property via exploring electrophoretic assembly dynamics

Xiaogang Guo[1,*] ⓘ, Taotao Liang[2,*], Guixiu Liu[1], Yuanzhen He[1], Shuying Kong[1], Md. Labu Islam[1], and Binfang Yuan[1]

[1] *Chongqing Key Laboratory of Inorganic Special Functional Materials, College of Chemistry and Chemical Engineering, Yangtze Normal University, Chongqing 408100, China*
[2] *Department of Orthopedic Surgery, Southwest Hospital, Chongqing Sports Medicine Center, The Third Military Medical University, Chongqing 40038, China*

ABSTRACT

Achieving controllable film-forming process is always a difficult issue for practical application, especially for bi-/multiple component composite materials. Thus, this paper firstly developed a conveniently and controllable electrophoretic assembly technique under mild conditions to design nano-Al-doped@Co₃O₄ energetic film with wide potential applications. The stable suspension consists of isopropyl alcohol with the tracing of polyethylenimine and tween 80. The high crystallinity and uniformity of structure in target films were demonstrated by FESEM, EDX, XRD, and FT-IR techniques. Electrophoretic assembly dynamics of Al/Co₃O₄ particles were deeply explored to provide a theoretical foundation for optimizing exothermic performance. The exothermic performance of target film can be accurately adjusted, and the output of heat (Q) and activation energy (E_a) can reach up to ~ 3.6 kJ/g (close to 85% of theoretical value) and low to 230.01 kJ/mol, respectively. This breakthrough will substantially push forward the facile functional film-forming process of different kinds of particles used in fields of electronics, military, aviation, etc.

Xiaogang Guo and Taotao Liang contributed equally to this work.

Address correspondence to E-mail: guoxiaogang0528@126.com; liangtaotao2018@foxmail.com

1 Introduction

During last decade, metastable intermixed composites (MICs) with superior self-contained heat-release capacity, usually composed of fuel-Al or Mg and oxidizing agent (B_2O_3, CuO, Fe_2O_3, etc.) [1–3], have attracted increasing attentions widely used in fields of sensors, detonators, triggers, and electronics [4–7]. The MICs with promising nanostructures have shown great advantages in increasing the contact area, shortening mass transfer distance, and improving the heat flow efficiency during the exothermic process. Until now, the current research emphases and difficulties of MICs have always been mainly focused on the development of uniform distribution, exploration of their film-forming technique, and precise control of components to optimize their thermopositive property.

With a high adiabatic reaction temperature of 3201 K [8], the Al-doped Co_3O_4 MIC, as a desirable energetic system, has been a valuable research focus. The theoretical heat-release (Q) of it can reach up to 4.2 kJ/g [9], much higher than that of other common systems (e.g. Al-doped CuO MIC, Al-doped Fe_2O_3 MIC), showing wide potential applications. Recently, various fabrication techniques, including magnetron sputtering [10], traditional sintering process [11], mechanical mixing method [12], and vapor deposition method [13], have been applied to design Al-doped Co_3O_4 MIC with different structures to improve its exothermicity. In fact, it is increasingly essential to construct energetic films or coatings based on Al-doped Co_3O_4 MICs when they are integrated with devices, electrodes, and substrates with complex shapes. However, because of the difficulties of reducing the preparation cost and improving preparation efficiency simultaneously, there are still bulging bottlenecks of facile fabrication of Al-doped Co_3O_4 MIC films, though relatively successful techniques or methods have been explored conducted by researchers. For example, the novel 3D-Al/Co_3O_4 nanothermite film was fabricated by magnetron sputtering deposition of nanoscale Al layers on Co_3O_4 porous skeletons substrate, showing a great heat-release property (1.7 kJ/g) and a violent deflagration process after a capacitor discharge stimulation [14]. Yang group demonstrated the feasibility of using thermal evaporation technique of Al to construct Al/Co_3O_4 MICs on a silicon substrate, possessing relatively uniform microstructure and great exothermicity with Q of 3.2 kJ/g [15]. In addition, Volochaev et al. reported the layered Co_3O_4/Al films fabricated using sequential reactive magnetron sputtering of a metallic Co target and Al target in a mixture gas of argon and oxygen, and pure argon gas, respectively, and further studied structural and magnetic properties of reaction product-Co/Al_2O_3 coatings after vacuum annealing treatment [16]. Thus, it is urgent to develop a controllable and convenient technique to solve mentioned issues.

Because of the outstanding advantages of simplicity, high versatility, and efficiency [17–20], an electrophoretic assembly technique has turned out to be a promising technique to construct various functional films from charged particles or molecules. Several energetic systems (e.g., Al-doped Bi_2O_3 MICs [21], Al-doped CuO MICs [22], Al-doped ZnO MICs [23]) have been efficiently designed by the electrophoretic assembly process. In fact, Zhang et al. group reported the successful electrophoretic assembly process of Al-doped Co_3O_4 MIC coating using the dispersing agent of a mixture of ethanol, acetylacetone, and nitric acid [9]. However, the presence of acid inevitably reacts with the fuel-Al, and the heat-release capacity needs to be improved due to relative maldistribution of components. Thus, in this paper, a developed electrophoretic assembly technique was proposed to design uniformly distribute Al-doped Co_3O_4 MIC film with enhanced exothermic performance. The suitable dispersing agent consisted of isopropanol, polyethylenimine, and tween 80. The electrophoretic assembly kinetic models of Al, Co_3O_4, and Al/Co_3O_4 particles were firstly built to adjust and control the intensity of exothermic reactions. Finally, the heat-release performance of all samples was also investigated.

2 Experimental section

2.1 Reagents and materials

Polyethylenimine (PEI), cobalt oxide, tween 80 were purchased from Aladdin Industrial Corporation. (Shanghai, China). The isopropyl alcohol (IPA) was purchased from Kelong Industrial Inc., China, and nano-Al (99.9%) particles were commercially available stored in a vacuum drying oven to protect it from oxidation. Other reagents (e.g., ethanol) bought

from Sinopharm Chemical Reagent Co., Ltd. were used without further purification. Double distilled (DD) water was used in all experiments. PEI used in this study needs to be diluted 100 times by ethanol. Ti sheets (99.9%) were used as working and counter electrodes during the controllable electrophoretic assembly process.

2.2 Controllable Design of Nano-Al-doped@Co$_3$O$_4$ Energetic Film

The schematic diagram of the design of nano-Al-doped@Co$_3$O$_4$ energetic film was shown in Fig. 1. After a comparative analysis of a large number of experiments using a series of suspending agents (ethanol, methanol, propanol, toluene, formaldehyde, etc.), the nano-Al-doped@Co$_3$O$_4$ energetic film was only successfully fabricated in the optimized IPA. Thus, the stable suspension can be obtained by the following two steps of (i) adding the Al and Co$_3$O$_4$ particles with different moral ratios into a mixture of 100 mL IPA + 1 mL tween 80 with the particle loading concentrations of 1–2 g/L and followed by ultrasonic treatment for 20 min at 25 °C and (ii) adding the trace PEI (2 mL) into the previous suspension to realize the surface modification of Al and Co$_3$O$_4$ particles and followed by the ultrasonic treatment for 10 min at 25 °C. Before electrophoretic assembly, the working and counter electrodes with

an effective contact area of 2×3 cm^2 were polished by sandpapers, ultrasonically cleaned in ethanol and DD water, and dried in a vacuum drying chamber in sequence. The mole ratio of nano-Al and Co$_3$O$_4$ in suspension ($\Phi_{S(AlCo_3O_4)}$) were adjusted by accurately weighing via a high precision electronic balance with an accuracy of 10^{-4} g. During electrophoretic assembly process, the distance of two electrodes was controlled at 1 cm, and charged particles were directly moved to the working electrode under different applied voltages from 5 to 25 V/mm at normal pressure and 25 °C. After electrophoretic assembly for 0–20 fmin, the working electrode with the target energetic film was removed from the stable suspension, and followed by vacuum drying treatment at 85 °C for 1 h. The nano-Al-doped@Co$_3$O$_4$ energetic film was finally obtained after natural cooling. All experiments were repeated in triplicate.

2.3 Materials characterization

The crystalline composition of product was investigated by a X-ray diffractometer (XRD-6000, Shimadzu, ZD-3AX, Inc., Japan) at a scanning rate of 4°/min equipped with Cu Kα radiation ($\lambda = \sim 0.15$ nm). The micro-morphologies of product were analyzed by field emission scanning electron microscope (FESEM, HITACHI SU5000+, Oxford Instruments Ultim Max, Japan) equipped
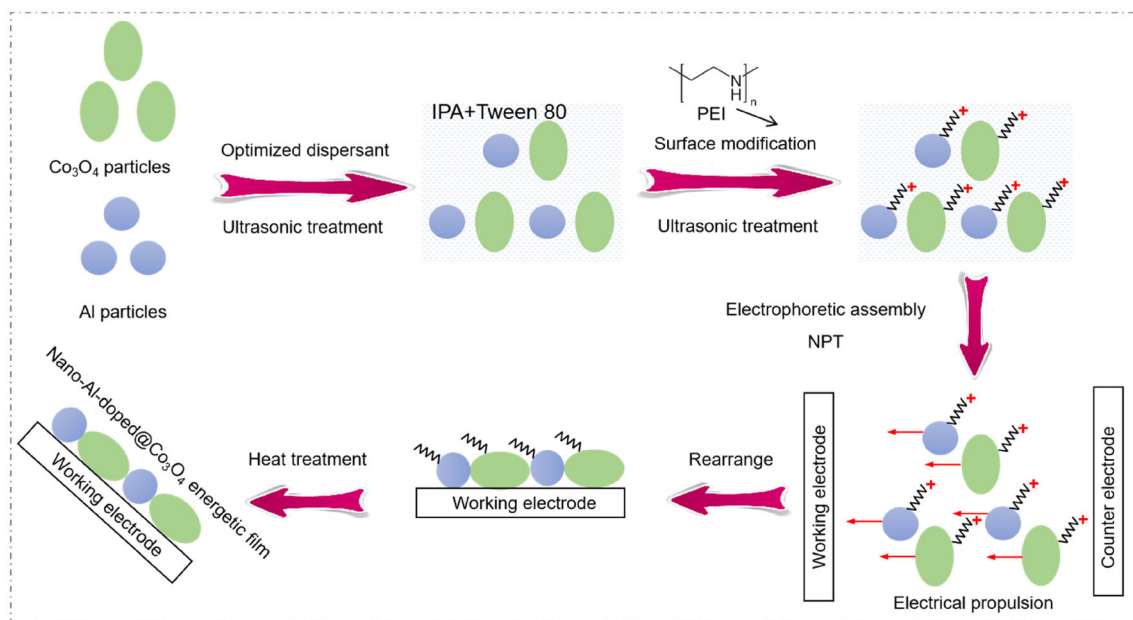

Fig. 1 Schematic diagram of the facile design of promising nano-Al-doped@Co$_3$O$_4$ energetic film

with the energy dispersive X-ray spectroscopy (EDX). The mole ratios of Al and Co_3O_4 in the product were determined by atomic absorption spectrometer (AAS, 180-80, Exter Analytical spectrograph, USA). The nano-Al-doped@Co_3O_4 energetic film was scraped off from the working electrode and characterized by differential scanning calorimetry (DSC) using a thermogravimetric analyzer (NETZSCH, STA449F3, Germany) from 25 to 1000 °C under Ar 99.999% atmosphere to analyze its heat-release property.

3 Results and discussion

3.1 Morphology and crystal structure characterization

Figure 2a displays the XRD pattern of the nano-Al-doped@Co_3O_4 energetic film prepared by the efficiently electrophoretic assembly. The characteristics of the spatial symmetry aluminum crystal structure are demonstrated by the orientations along the Al (111), Al (200), Al (220), and Al (311) directions at the corresponding diffraction angle of 38.472°, 44.738°, 65.133°, and 78.227°, which is accorded with the standard pattern for pure Al (PDF# Card No.

04-0787). While the other peaks are assigned to Co_3O_4 (PDF# card No. 43-1003, $Fd3m$(227)) with crystal lattice parameters of $a = b = c = 8.084$ Å. Meanwhile, sharp peaks of obtained Co_3O_4 and Al crystals indicate that they are highly crystallized, and there are no other peaks (Al_2O_3, Co, etc.) in Fig. 2a, indicating the high purity of product and no chemical reaction during electrophoretic assembly process. Thus, these results also demonstrate the superiority of electrophoretic assembly to design nano-Al-doped@Co_3O_4 energetic film in the stable suspension. The surface morphology of the target film was analyzed by FESEM technique in Fig. 2b–d. Clearly, sample surface is uniformly distributed with rare locally reunion areas in low-resolution FESEM image of Fig. 2b. Moreover, nano-Al particles randomly scattered in the Co_3O_4 matrix in a high magnification FESEM image of target film in Fig. 2c, where it is found that there are still some cracks also clearly seen in Fig. 2d. The presence of tiny cracks acted as heat flow release channels provide the promising structural foundation to improve the sufficient degree of exothermic reaction. In addition, as shown in partial enlarged higher magnification FESEM image (Fig. 2d), Al particles are still in nanoscale, contributing to increasing the reaction contact area and

Fig. 2 a The typical XRD pattern of nano-Al-doped@Co_3O_4 energetic film, and the FESEM (low-resolution (b) and high-resolution (c)) images of product, and d partial enlarged image of blue dotted area in (c)
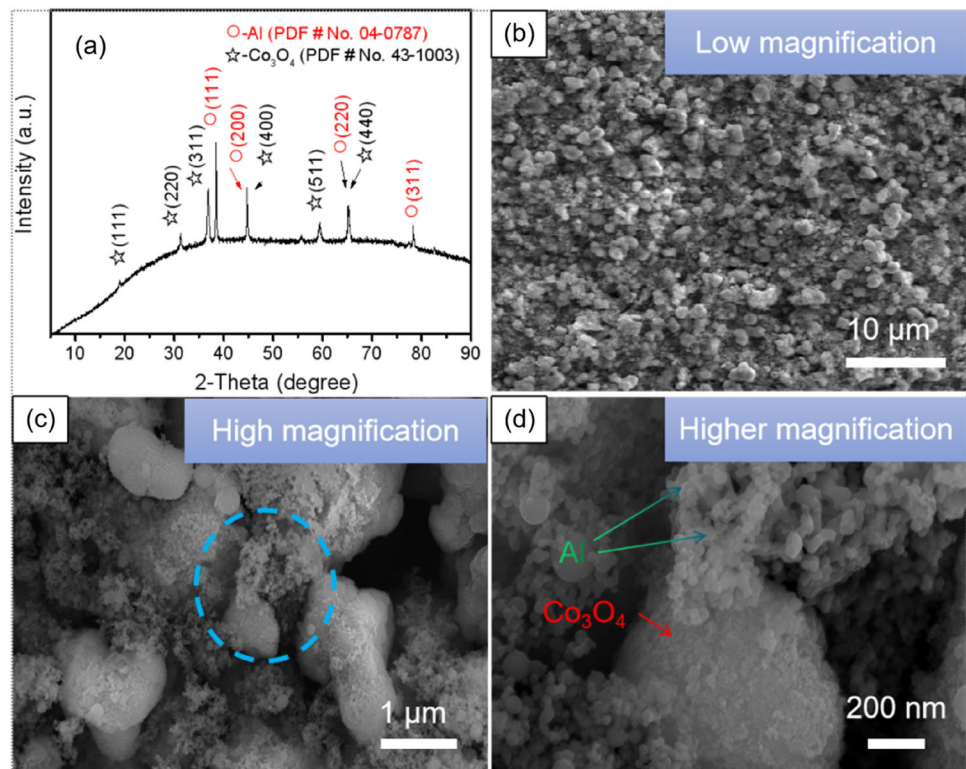
shortening the mass transfer distance during the heat-release process.

In addition, top-view FESEM images along with elemental mapping and EDX spectrums for product were displayed in Fig. 3. The entire region in the top-view image (Fig. 3a, b) corresponds to the elemental mapping region. Uniformity of product was also demonstrated by the distribution diagrams of all key elements of Al, Co, and O in two random regions. The Ti element is from the substrate. For two random regions, the signal peaks of all elements are clearly displayed in EDX spectrums in Fig. 3c, d. Furthermore, the mole percent of these elements are analyzed in Fig. 3c, d, which is 26.9%:31.4%:40.9%:∼1% and 27.1%:31.3%:41.0%:∼1% for Al:Co:O:Ti of samples in two random regions, and the calculated mole ratio of key elements of Al:Co:O is close to 8:9:12 of theoretical reaction ratio of $Al@Co_3O_4$ energetic system. Moreover, the similar results are also verified by AAS technique (Table 1). Moreover, the mole ratio of Al to Co_3O_4 in product ($\Phi_{p(AlCo_3O_4)}$) shows an almost linear relationship with $\Phi_{S(AlCo_3O_4)}$ demonstrated by EDX and AAS technique (Fig. 4), further demonstrating the high controllability of element content within target energetic film via electrophoretic assembly technique.

3.2 Electrophoretic assembly dynamic studies

Generally, the film-forming process of different particles during electrophoretic assembly is a kinetically driven process [24]. In this study, for electrophoretic assembly of energetic film, the key evaluation criterion for a desirable stable dispersion system was that the surface of both fuel-Al and Co_3O_4 particles can be efficiently modified by the same electric charge in a stable suspension.

Figure 5 shows the zeta potentials of Al, Co_3O_4 and Al/Co_3O_4 particles as functions of the concentration of PEI as a highly effective surface modifier with lots of branched molecules [25]. There are scarcely any deposits on the working electrode substrate without the addition of PEI. The zeta potentials of Al, Co_3O_4 and Al/Co_3O_4 particles increase sharply with increased concentration of PEI, and reach to the peak value as the concentration of PEI is around 2 mL/100 mL, and then decrease slightly, respectively. That is mainly due to the increased flocculation and
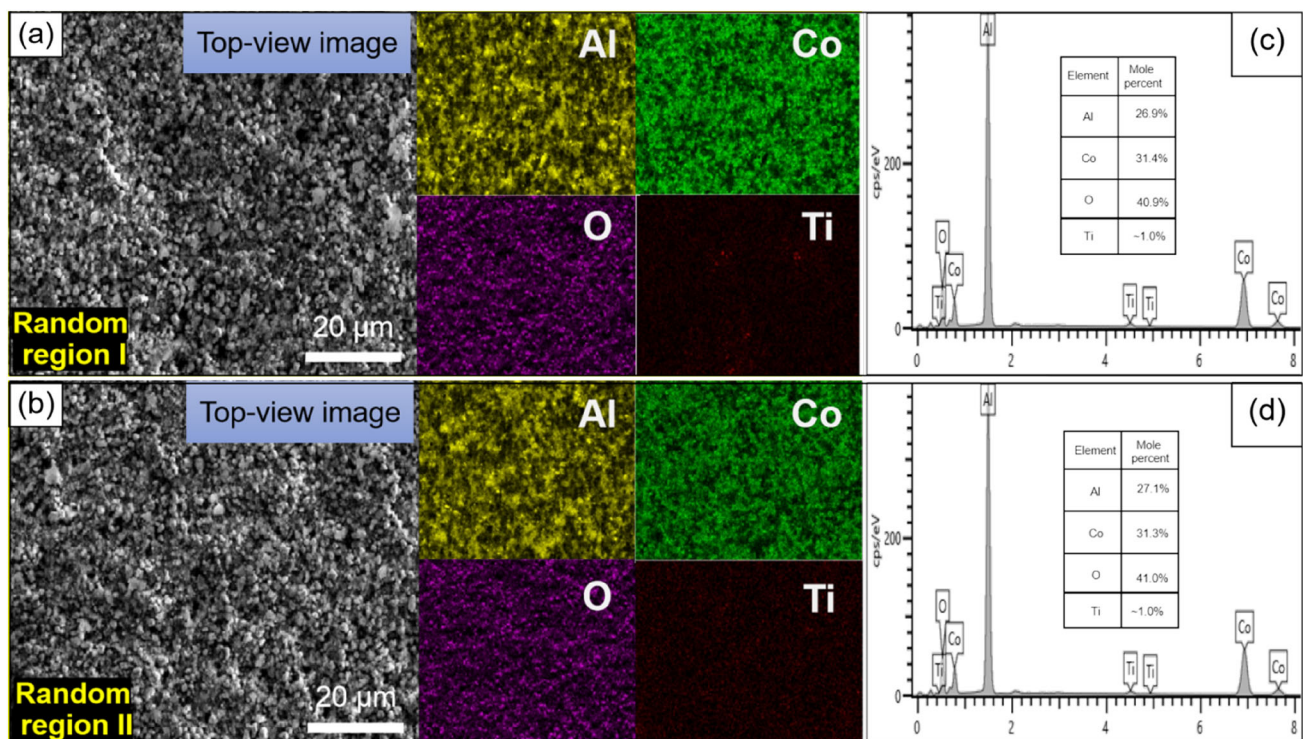

Fig. 3 a Top-view image of the sample in the random region I (a) and II (b) with the respective elemental mapping, followed by the EDX spectrums of the samples in region I (c) and II (d)

Table 1 Summary of the mole ratios of nano-Al-doped@Co_3O_4 energetic film

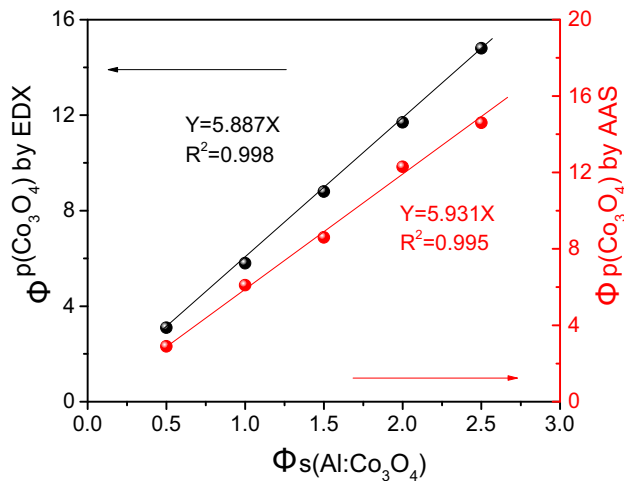| Element	Mole percent by EDX (%)	Mole percent by AAS (%)
Al	26.9	27.1
Co	31.4	30.0
O	40.9	42.9
Ti	∼ 1	–

Fig. 4 The $\Phi_{p(AlCo_3O_4)}$ as functions of the $\Phi_{S(AlCo_3O_4)}$ determined by EDX and AAS technique
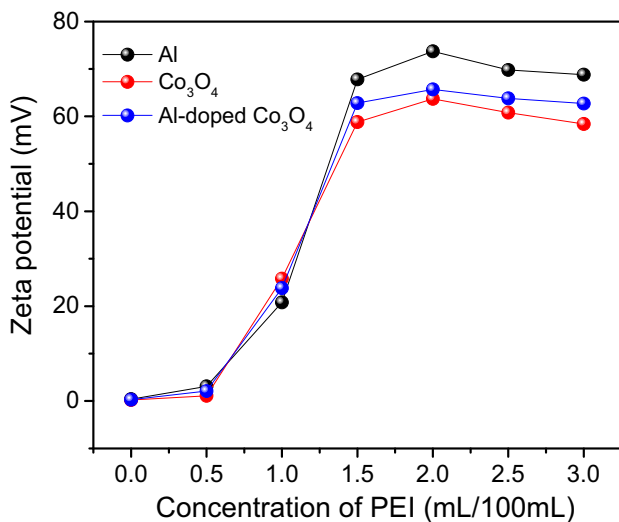

Fig. 5 Effect of PEI concentrations on the zeta potentials of Al, Co_3O_4 and Al/Co_3O_4 particles

sedimentation rate of the charged Al and Co_3O_4 particles after adsorbing excessive PEI. Thus, the concentration of PEI is controlled at 2 mL/100 mL to obtain the stable suspension with the highest zeta potential for the following highly-efficient

electrophoretic assembly process of nano-Al-doped@Co_3O_4 energetic film.

The electrophoretic assembly dynamics of Al and Co_3O_4 particles deposited on the working electrode are further explored in Fig. 6. It is clearly seen that the electrophoretic assembly efficiency of Al increases linearly with electrophoretic assembly time ($T < 8$ min) (Fig. 6a), that is, the first time period (0–8 min) is the linear control stage for Al particles with the linear fitting formula (Eq. 1) as follows:

$$Y_{Al} = 0.511X, \quad (0 < X < 8\,\text{min}, \ R^2 = 0.999) \quad (1)$$

where Y_{Al} and X are the electrophoretic assembly efficiency (mg/cm^2) and electrophoretic assembly time (min). The result is in accord with the research by Wang et al. [26]. In general, electrophoretic assembly process of particles has two kinds of kinetic behaviors of linear and non-linear or parabolic deposition kinetic. For the linear deposition kinetic within a relatively short deposition time (t), electrophoretic assembly efficiency increases linearly with the time, and the model expression can be expressed as (Eq. 2) under a certain applied voltage. For the non-linear deposition kinetic, the electrophoretic assembly efficiency increases linearly with $t^{0.5}$ as the electrophoretic assembly time continues to increasing, and the corresponding model can be expressed as (Eq. 3):

$$Y = \frac{\varepsilon C \zeta}{4\pi\eta}(E - \Delta E)t \quad (2)$$

$$Y = 2\frac{\varepsilon C \zeta}{4\pi\eta}(E - \Delta E)t_m^{0.5}e^{-kt_m}t^{0.5} + \frac{\varepsilon C \zeta}{4\pi\eta}(E - \Delta E)b \quad (3)$$

where the $Y, \varepsilon, C, \eta, \zeta, E, \Delta E, t_m$ and b is the electrophoretic assembly efficiency, dielectric constant of dispersed medium, solids loading in suspension, the viscosity of dispersed medium, the zeta potential of the particle, applied field strength, the field drop in field along the direction of the assembly, the key time between linear and non-linear control stage, and the constant. In this study, with the assembly time increasing from the t_m (8 min), a non-linear
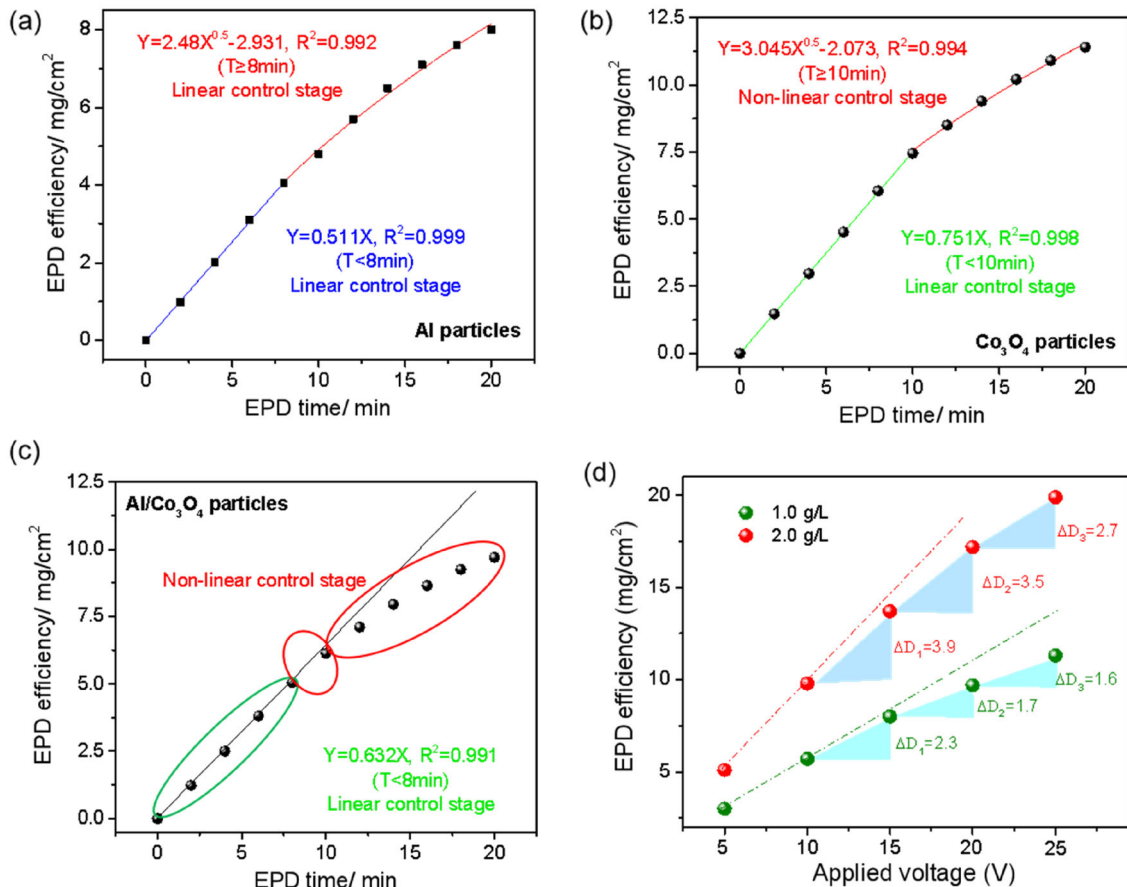
Fig. 6 a Variation of electrophoretic assembly deposition (EPD) efficiency with deposition time during electrophoretic assembly process of Al (**a**), Co_3O_4 (**b**), Al/Co_3O_4 (**c**) particles, and **d** the electrophoretic assembly efficiency as functions of applied voltage in different loading concentrations

relationship between electrophoretic assembly efficiency and time is observed in Fig. 6a. Clearly, electrophoretic assembly efficiency (Y, mg/cm²) increases linearly with $X^{0.5}$, the fitted relational expression (Eq. 4) is as follows:

$$Y = 2.48X^{0.5} - 2.931, (X \geq 8\, min, R^2 = 0.992) \qquad (4)$$

Similar electrophoretic assembly behaviors can be observed for Co_3O_4 (Fig. 6b). For Co_3O_4 particles in the linear control stage:

$$Y_{Co_3O_4} = 0.751X, \quad (< X < 10\, min, R^2 = 0.998) \qquad (5)$$

For Co_3O_4 particles in the non-linear control stage:

$$Y_{Co_3O_4} = 3.045X^{0.5} - 2.073, (X \geq 10\, min, R^2 = 0.994) \qquad (6)$$

However, the t_m for Co_3O_4 is 10 min longer than that for Al particles. The reason is probably due to the stronger charge pack capacity for Co_3O_4 than that for

Al nanoparticles. Thus, as shown in Fig. 6c, for Al/Co_3O_4 particles, the electrophoretic assembly efficiency still increases linearly with assembly time before 8 min (Eq. 7), and the linear change does not apply for a prolonged deposition.

$$Y_{Al/Co_3O_4} = 0.632X, (0 < X < 8\, min, R^2 = 0.991) \qquad (7)$$

The mole ratio of Al to Co_3O_4 in product ($\Phi_{p(AlCo_3O_4)}$), essential to output performance, can be determined by co-deposition kinetic study (Fig. 6c). For 0 8 min, $\Phi_{p(AlCo_3O_4)}$ can remain a constant value, which can be expressed as Eq. 8. For 8–10 min, and a longer assembly time (> 10 min), the $\Phi_{p(AlCo_3O_4)}$ shows a relative relatively complex change relationship with assembly time, which can be expressed as Eqs. 9 and 10. In fact, it is essential to realize the accurate control for a codeposition of Al and Co_3O_4, and the electrophoretic assembly time is determined at 8 min in the linear control stage.

Fig. 7 **a** DSC curves of nano-Al-doped@Co_3O_4 energetic film fabricated by electrophoretic assembly for 8–12 min, and **b** DSC curves of samples with different $\Phi_{p(AlCo_3O_4)}$
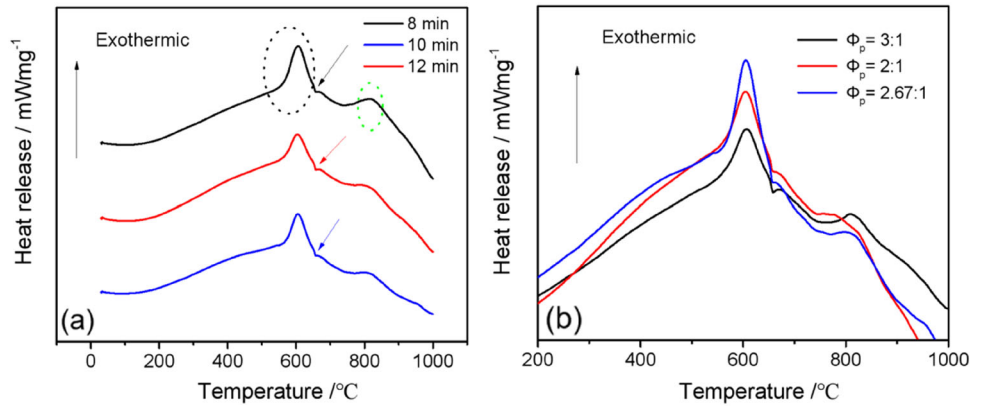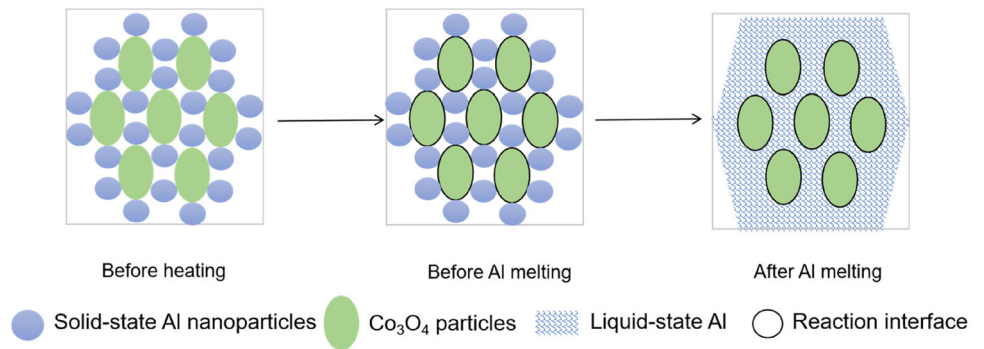
Fig. 8 Schematic illustrations of the transformation process of reaction interfaces before and after Al melting

$$\Phi_{p(Al:Co_3O_4)} = \frac{0.511 M_{Co_3O_4}}{0.751 M_{Al}}, \quad (<X<8\,\text{min}) \quad (8)$$

$$\Phi_{p(Al:Co_3O_4)} = \frac{(2.48X^{0.5} - 2.931)M_{Co_3O_4}}{0.751 M_{Al}}, (8 \leq X \leq 10\,\text{min}) \quad (9)$$

$$\Phi_{p(Al:Co_3O_4)} = \frac{(2.48X^{0.5} - 2.931)M_{Co_3O_4}}{(3.045X^{0.5} - 2.073)M_{Al}}, \quad (10)$$
$$(X > 10\,\text{min})$$

In addition, electrophoretic assembly efficiency as a function of applied voltage is displayed in Fig. 6d. The difference of electrophoretic assembly efficiency of sample at 5 V/mm intervals is defined as ΔD, and the ΔD_1, ΔD_2, and ΔD_3 is the difference of electrophoretic assembly efficiency as voltage changes from 10 to 15 V, 15 to 20 V, 20 to 25 V/mm, respectively. Clearly, for the particle concentration of 1 g/L, electrophoretic assembly efficiency increases almost linearly as the applied voltage is lower than 10 V/mm. The growth rate slows down with voltage continues to increasing probably due to more intensified collision among particles and a more pronounced sedimentation process under a higher voltage, and the corresponding ΔD gradually decreases with ΔD_1

(2.3) > ΔD_2 (1.7) > ΔD_3 (1.6), which demonstrates the over-voltage will goes against the high efficiency electrophoretic assembly. There is a similar change law of electrophoretic assembly efficiency and voltage for higher particles concentration of 2 g/L. However, each difference value (ΔD) of electrophoretic assembly efficiency in a certain voltage change range for particles concentration of 2 g/L is higher than that of 1 g/L (Fig. 6d), probably due to the synergistic effect of a greater degree of sedimentation of particles, more violent collision among particles, and decreased solution concentration in suspension, etc. [21, 27, 28].

3.3 Heat-release performance analysis

The heat-release performance of nano-Al-doped@Co_3O_4 energetic film is deeply explored by DSC technique in Fig. 7. For sample obtained by electrophoretic assembly for 8 min, the DSC curve increases sharply to maximum value as the heat temperature in Ar atmosphere is ~ 605 °C due to the intense heat-release reaction (Eq. 11) shown in Fig. 7a (black dotted-line circle).

$$8Al + 3Co_3O_4 \rightarrow 4Al_2O_3 + 9Co, \Delta Q = 4237 J/g \qquad (11)$$
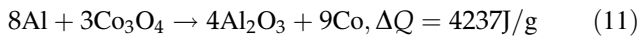
The lower onset temperature of ca. 550 °C shows the outstanding detonation advantage compared with that of 955 °C and 1040 °C for aluminum/molybdenum trioxide and aluminum/copper oxide [13]. What is noteworthy is that a tiny endothermic peak at $\sim$ 660 °C can not be ignored due to the melting process of Al particles [15]. In addition, there is another weak exothermic peak at around 800 °C mainly because of heat-release reaction of solid Co_3O_4 particles and liquid-state-Al in Fig. 7a (green dotted-line circle). In this state, the reaction interface changes from solid-Al@solid-Co_3O_4 to solid-Co_3O_4@liquid-Al (Fig. 8), and the reaction contact area greatly increased, which further speeds up the reaction process. The total output of heat (Q) is ca. 85% of theoretical value of $\sim$ 3.6 k J/g by simulation analysis software. In addition, samples obtained by electrophoretic assembly for 10 min and 12 min shows similar DSC curves though the respective Q is ca. 92% and 87% of that for 8 min (Fig. 7a), which is probably due to the inadequate exothermic reaction.

Moreover, the DSC curves of product with different $\Phi_{p(AlCo_3O_4)}$ adjusted by electrophoretic assembly dynamics of Al/Co_3O_4 particles are similar showed in Fig. 7b. The Q of sample with $\Phi_{p(AlCo_3O_4)}$ of 2.67:1 (close to the theoretical reaction ratio of 8:3) is highest compared with that of 2:1 and 3:1. Thus, exothermic performance of samples can be flexibly controlled by adjusting the $\Phi_{S(AlCo_3O_4)}$ and electrophoretic assembly dynamics. The activation energy (E_a) of samples is also calculated via Kissinger Akahira–Sunose method (Eq. 12) [29]

$$\ln\left(\frac{\beta}{T_P^2}\right) = \ln\left(\frac{RA}{E_a}\right) - \frac{E_a}{RT_P} \qquad (12)$$

where E_a, β, R, T_P, and A is the activation energy, the value of the linear heating rate (K/min), the universal constant as 8.314 J/(mol K), the value of peak absolute temperature (K), and the pre-exponential factor (s^{-1}). The heating rates are selected as 10, 20, 30, and 40 K/min, respectively. Combined with DSC curves, the E_a value of samples prepared by electrophoretic assembly for 8 min is low as 230.01 kJ/mol, indicating a small activation energy barrier to overcome, and contributing to easily rapid release of heat energy, and further providing great potential applications for designing other composite energetic systems.

4 Conclusion

In summary, the novel nano-Al-doped@Co_3O_4 energetic film with promising even microstructure distribution and superior performance was conveniently fabricated via a controllable electrophoretic assembly. Target film possesses high purity and crystallinity determined by XRD, FESEM, and EDX. Electrophoretic assembly dynamics of Al/Co_3O_4 particles were deeply explored, which turned out to be a control bridge to connect the $\Phi_{S(AlCo_3O_4)}$ and $\Phi_{p(AlCo_3O_4)}$ to largely optimize heat-release performance. The DSC results indicated that there was an intense exothermic process with 85% of theoretical output of heat once the reaction of fuel-Al and oxidizing agent in obtained energetic film with low activation energy (E_a) was triggered. Thus, it is believed that this study creatively opens a novel view-sight and provides a valuable reference to design other electrophoretic assembly of bicomposites with various wide applications.

Author contributions

XGG designed experiments, and wrote the first draft of the manuscript and conducted the research. GXL, YZH, and MLI performed all surface characterization and contributed to the interpretation of the surface analysis. SYK and BFY completed the data optimization analysis. TTL contributed to the writing of the manuscript and approved the final version of it.

Data availability

The authors declare that all data supporting the findings of this study are available within the article.

Declarations

Conflict of interest The authors declare that they have no known competing financial interests or personal relationships that could have appeared to influence the work reported in this paper.

References

1. Y.G. Xu, Q. Wang, C. Shen, Q.H. Lin, P.C. Wang, M. Lu, A series of energetic metal pentazolate hydrates. Nature **549**, 78 (2017)
2. W. He, P.J. Liu, G.Q. He, M. Gozin, Q.L. Yan, Highly reactive metastable intermixed composites (MICs): preparation and characterization. Adv. Mater. **30**, 1706293 (2018)
3. X.X. Ma, Y.X. Li, I. Hussain, R.Q. Shen, G.C. Yang, K.L. Zhang, Core-shell structured nanoenergetic materials: preparation and fundamental properties. Adv. Mater. **32**, 2002091 (2020)
4. S.H. Feng, G.L. Xiong, W.H. Zhu, Ab initio molecular dynamics studies on the ignition and combustion mechanisms, twice exothermic characteristics, and mass transport properties of Al/NiO nanothermite. J. Mater. Sci. **56**, 11364 (2021)
5. M. Yang, J.X. Liu, S.K. Li, S. Zhang, Y.C. Wang, C. He, Ultrafast synthesis of graphene nanosheets encapsulated Si nanoparticles via deflagration of energetic materials for lithium-ion batteries. Nano Energy **65**, 104028 (2019)
6. X.G. Guo, X.M. Li, C. Lai, X. Jiang, X.M. Li, Y.J. Shu, Facile approach to the green synthesis of novel ternary composites with excellent superhydrophobic and thermal stability property: an expanding horizon. Chem. Eng. J. **309**, 240 (2017)
7. A.N. Streletskii, I.V. Kolbanev, G.A. Vorobieva, A.Y. Dolgoborodov, V.G. Kirilenko, B.D. Yankovskii, Kinetics of mechanical activation of Al/CuO thermite. J. Mater. Sci. **53**, 13550 (2018)
8. F. Xiao, J.M. Li, X.Y. Zhou, R.J. Yang, Preparation of mechanically activated aluminumrich Al-Co$_3$O$_4$ powders and their thermal properties and reactivity with water steam at high temperature. Comust. Sci. Technol. **190**, 1935 (2018)
9. D.X. Zhang, Q. Xiang, Electrophoretic fabrication of an Al/Co$_3$O$_4$ reactive nanocomposite coating and its application in a microignitor. Ind. Eng. Chem. Res. **55**, 8243 (2016)
10. Z.J. Liu, B. Hu, D.L. Li, P. Zhu, Y.H. Ye, R.Q. Shen, Preparation and characterization of Co$_3$O$_4$/Al core-shell nanoenergetic materials and their application in energetic semiconductor bridges. Eur. Phys. J. Appl. Phys. **72**, 30401 (2015)
11. R. Kiahosseini, H. Ahmadian, Effect of residual structural strain caused by the addition of Co$_3$O$_4$ nanoparticles on the structural, hardness and magnetic properties of an Al/Co$_3$O$_4$ nanocomposite produced by powder metallurgy. Int. J. Min. Met. Mater. **27**, 384 (2020)
12. Y.F. Liu, J.L. Xie, M. Luo, S. Jian, B. Peng, L.J. Deng, The synthesis and characterization of Al/Co$_3$O$_4$ magnetic composite pigments with low infrared emissivity and low lightness. Infrared Phys. Techn. **83**, 88 (2017)
13. D.G. Xu, Y. Yang, H. Cheng, Y.Y. Li, K.L. Zhang, Integration of nano-Al with Co$_3$O$_4$ nanorods to realize high-exothermic core-shell nanoenergetic materials on a silicon substrate. Combust Flame **159**, 2202 (2012)
14. Z.L. Zheng, W.C. Zhang, C.P. Yu, G.Q. Zheng, K.F. Ma, Z.C. Qin, J.H. Ye, Y.M. Chao, Integration of the 3DOM Al/Co$_3$O$_4$ nanothermite film with a semiconductor bridge to realize a highoutput micro-energetic igniter. RSC Adv. **8**, 2552 (2018)
15. J. Wang, Z.Q. Qiao, J.P. Shen, R. Li, Y.T. Yang, G.T. Yang, Large-scale synthesis of a porous Co$_3$O$_4$ nanostructure and its application in metastable intermolecular composites. Propellants Explos. Pyrotech. **50**, 514 (2015)
16. M.N. Volochaev, S.V. Komogortsev, V.G. Myagkov, L.E. Bykova, V.S. Zhigalov, N.P. Shestakov, D.A. Velikanov, D.A. Smolyakov, A.V. Luk'yanenko, V.B. Rachek, Y.Y. Loginov, I.A. Tambasov, A.A. Matsynin, Structural and magnetic characteristics of nanogranular Co-Al$_2$O$_3$ single- and multi-layer films formed by the solid-state synthesis. Phys. Solid State **60**, 1425 (2018)
17. Q. Nawaz, S. Fastner, M.A.U. Rehman, S. Ferraris, S. Perero, G.G. Confiengo, E. Yavuz, M. Ferraris, A.R. Boccaccini, Multifunctional stratified composite coatings by electrophoretic deposition and RF co-sputtering for orthopaedic implants. J. Mater. Sci. **56**, 7920 (2021)
18. F. Praetorius, B. Kick, K.L. Behler, M.N. Honemann, D. Weuster-Botz, H. Dietz, Biotechnological mass production of DNA origami. Nature **552**, 84 (2017)

19. I. Hod, W. Bury, D.M. Karlin, P. Deria, C.-W. Kung, M.J. Katz, M. So, B. Klahr, D. Jin, Y.-W. Chung, T.W. Odom, O.K. Farha, J.T. Hupp, Directed growth of electroactive metal-organic framework thin films using electrophoretic deposition. Adv. Mater. **26**, 6295 (2014)

20. F. Lin, S.W. Boettcher, Adaptive semiconductor/electrocatalyst junctions in water splitting photoanodes. Nat. Mater. **13**, 81 (2013)

21. X.G. Guo, C. Lai, X. Jiang, W.H. Min, Y.J. Yin, X.L. Li, Y.J. Shu, Remarkably facile fabrication of extremely superhydrophobic high-energy binary composite with ultralong lifespan. Chem. Eng. J. **335**, 240 (2018)

22. K.T. Sullivan, C. Zhu, E.B. Duoss, A.E. Gash, D.B. Kolesky, J.D. Kuntz, J.A. Lewis, C.M. Spadaccini, Controlling material reactivity using architecture. Adv. Mater. **28**, 1934 (2016)

23. X.G. Guo, T.T. Liang, J. Wang, X.M. Li, Facilely electrophoretic derived aluminum/zinc (II) oxide nanocomposite with superhydrophobicity and thermostability. Ceram. Int. **46**, 1052 (2020)

24. H. Zhang, C. Kinnear, P. Mulvaney, Fabrication of single-nanocrystal srrays. Adv. Mater. **2**, 1904551 (2020)

25. F.Q. Tang, T. Uchikoshi, K. Ozawa, Y. Sakka, Effect of polyethylenimine on the dispersion and electrophoretic deposition of nano-sized titania aqueous suspensions. J. Eur. Ceram. Soc. **26**, 1555 (2006)

26. Y.C. Wan, I.C. Leu, M.H. Hon, Kinetics of electrophoretic deposition for nanocrystalline zinc oxide coatings. J. Am. Ceram. Soc. **87**, 84 (2014)

27. H. Hadraba, D. Drdlik, Z. Chlup, K. Maca, I. Dlouhy, J. Cihlar, Layered ceramic composites via control of electrophoretic deposition kinetics. J. Eur. Ceram. Soc. **33**, 2305 (2013)

28. X.G. Guo, X.M. Li, H.R. Li, D.X. Zhang, C. Lai, W.L. Li, A comprehensive investigation on the electrophoretic deposition (EPD) of nano-Al/Ni energetic composite coatings for the combustion application. Surf. Coat. Technol. **265**, 83 (2015)

29. F. Yang, G.C. Yang, X.D. Yang, H.B. Bao, Y.J. Yang, X.G. Guo, Z.Q. Qiao, X.M. Li, Facile synthesis of high tightly ordered Al/CuO core-shell nanowire arrays and the effect of surface density on combustion. J. Alloys. Compd. **877**, 60025 (2021)